NASA CONTRACTOR REPORT

ELECTRON ATTACHMENT TO ATOMIC FLUORINE IN THERMALLY IONIZED AIR

by R. Earl Good

Prepared by
MITHRAS, INC.
Cambridge, Mass.
for

NATIONAL AERONAUTICS AND SPACE ADMINISTRATION • WASHINGTON, D. C. • JULY 1966

ELECTRON ATTACHMENT TO ATOMIC FLUORINE IN THERMALLY IONIZED AIR

By R. Earl Good

Prepared under Contract Nos. NASw-601 and NASw-941 by
MITHRAS, INC.
Cambridge, Mass.

for

NATIONAL AERONAUTICS AND SPACE ADMINISTRATION

For sale by the Clearinghouse for Federal Scientific and Technical Information
Springfield, Virginia 22151 – Price $3.00

FOREWORD

The research reported herein has been directed to the development of a plasma suppression technique for re-entry flight. This study is an experimental investigation of three-body electron attachment rates.

This research was sponsored under the Physics of Fluid Program of NASA Headquarters under contracts NASw-601 and NASw-941. This report covers work completed between June 1962 and June 1964.

The author wishes to express appreciation to Mr. Jacques A. F. Hill for his many helpful suggestions and to Mr. James Draper and Mr. David Stickler for their assistance in performing the experiments.

ABSTRACT

Fluorine gas is considered as a means of reducing the electron concentration during atmospheric re-entry. It is anticipated that the addition of fluorine gases to a re-entry plasma can alleviate radio communications blackout. The fluorine gases were investigated using a shock tube and wedge nozzle at throat conditions of 1 1/2 atmospheres and 3840°K. The fluorine gases, SF_6 and CF_4, were pre-mixed with air in the shock tube. The gases completely dissociated into atomic species prior to expanding into the nozzle and attaching electrons. Microwave interferometer measurements were made to determine the electron densities with and without fluorine gas additives. An Arrhenius type rate law was fit to the measurements of electron density to derive a rate coefficient for the fluorine attachment reaction.

TABLE OF CONTENTS

LIST OF ILLUSTRATIONS

1.0 INTRODUCTION

The air around a hypersonic vehicle is ionized and forms a plasma sheath which interfers with the radio frequency signals transmitted to and from the vehicle. The "radio blackout" reported during re-entry of the Mercury and Gemini spacecraft demonstrated that this interference caused by the plasma sheath can completely block communications between the vehicle and ground stations. On present orbital flights, radio blackout can be tolerated because it persists for only a few minutes. During future super-orbital re-entries or re-entries of lifting vehicles, however, the blackout will persist for much longer periods and may create a dangerous gap in communications.

In order to produce a communications "window" in the plasma sheath, electron density in the regions of the air flow surrounding the antenna or receiver on the vehicle must be reduced. The obvious way to reduce electron density is to cool the air flow, either by aerodynamic shaping or coolant injection. Unfortunately, the flow can be cooled without an accompanying reduction in the plasma ionization since the inherent electron recombination rate is too slow to achieve thermodynamic equilibrium anywhere near the point of coolant injection. For cooling to be effective, therefore, a means of speeding up the rate of electron removal is required. The coolant must serve either as a catalyst to enhance the recombination rate or as a "sink" to entrap free electrons through the use of such electrophilic substances as the halogen atoms Cl, F, Br or I.

Prior research by MITHRAS, Inc. has shown that many halogen compounds can be used which will both cool the flow by their dissociation into atoms and attach electrons to their dissociated atoms. The cooling capacity of the halogen compounds has been compared with that of helium and water in terms of the quantity of heat that can be absorbed per pound of coolant in raising the coolant to a specified temperature. Figure 1 shows that, on a equal weight basis, sulfur hexafluoride (SF_6) is more

efficient than water or helium. Thus, for example, the injection of SF_6 into a high temperature plasma will produce cooling through the dissociation of SF_6 into atoms and will achieve rapid electron removal through attachment to atomic fluorine.

The purpose of this study was to measure the rate of electron attachment to atomic fluorine. The equilibrium number of electrons that will attach to fluorine could be predicted from the known properties of the atom. The rate of attachment, however, could not be predicted and had not been measured previously. This report contains the results of the recent measurements conducted by MITHRAS, Inc. The measurements were conducted in a shock tube. The fluorine was added to the air in the shock tube as SF_6 or Freon-14 (CF_4). In the shock tube, the SF_6 and CF_4 were dissociated to leave atomic fluorine. The rate coefficient for three-body fluorine attachment was deduced from comparisons of measured electron densities with and without fluorine atoms. The technique, results, and analysis are described in the following pages.

2.0 SHOCK TUBE EXPERIMENTS

2.1 Basic Technique

The technique for measuring the electron attachment rate was to compare the electron density with and without the presence of fluorine. A small diameter shock tube was used to produce the ionized air which exhausted through a two-dimensional wedge nozzle. The test conditions in the shock tube were at a temperature of 3840°K and a pressure of 1 1/2 atmospheres. Fluorine was introduced into the shock tube as inert fluorine compounds; sulfur hexafluoride (SF_6) and Freon -14 (CF_4). The fluorine compounds were mixed with the air in the shock tube prior to firing. The firing of the shock tube produced a shock wave which dissociated the compounds into atomic species.

The fluorine compounds could be pre-mixed with the air because dissociation of the compounds occurred prior to the ionization of the air. The presence of small concentrations of atomic fluorine in the 3840°K ionized air did not alter the level of equilibrium ionization. It was necessary to cool the air to a temperature below 3000°K before electron attachment to fluorine became an important reaction.

To measure the electron attachment, the air was cooled by expansion through a 10 degree wedge nozzle. The expansion was too rapid to maintain equilibrium electron densities by recombination. Hence, the electron fraction "froze" and remained at a high level even though the air temperature cooled to a temperature below 3000°K. With the electron fraction frozen, the only change in the electron density is a volume change. The addition of fluorine atoms to the air altered this picture. The fluorine atoms attached electrons and conspicuously reduced the electron density.

The electron attachment rate was determined from electron density measurements made at various nozzle stations. With no fluorine present, the difference in electron density measured at two nozzle stations

represented the mass density change due to the nozzle area change. With fluorine added, there was an additional electron density change with was caused by electron attachment to the fluorine atoms. A Lagrangian transformation converted the electron density change with nozzle station to an electron attachment rate.

2.2 Dissociation of Additives

The dissociation of the additives used in these experiments was found to proceed to completion at the high temperatures and pressures created in the shock tube. At these high temperatures, the dissociated species are essentially inert. Consequently, the dissociation of SF_6 and CF_4 was described by the following general reaction:

$$AB_n \rightleftharpoons AB_{n-1} + B \qquad ; \; n = 1, \; 2 \qquad (2.1)$$

The fraction of dissociation occurring was determined from the equilibrium condition defined in terms of the equilibrium constant.

The equilibrium constant is defined as the ratio of the concentration of products over the concentration of reactants. For the dissociation reaction (2.1), the equilibrium constant is

$$K_c = \frac{(AB_{n-1})\,(B)}{(AB_n)} \qquad (2.2)$$

where the brackets represent molecules/cc. The equilibrium constant is related to the partition functions (see Reference 1) by:

$$\ell n \; K_c = - \frac{\Delta E_o}{T} + \sum_{i=i}^{n} \Delta\gamma_i \, \ell n \, Q\,(A_i) \qquad (2.3)$$

where $\Delta\gamma_i$ is the difference in the stoichiometric coefficients of the products and the reactants. The ΔE_o is the difference in the zero point energy between the products and the reactants; both referred to their standard states. The partition function is defined as the product of the

partition functions for translation, rotation, vibration, and electronic energy states. The partition function for translation (Q_t) and electronic states (Q_e), respectively, are given below:

$$Q_t = \left(\frac{2\pi mkT}{h^2}\right)^{3/2} \tag{2.4}$$

$$Q_e = \sum_{n=1}^{\infty} g_n \, e^{-\epsilon_n/kT} \tag{2.5}$$

where:

m	=	mass
k	=	Boltzmann's constant
h	=	Planck's constant
T	=	Temperature
g_n	=	Electron degeneracy
ϵ_n	=	Electron excitation level in atoms

The equilibrium constant for dissociation was estimated as

$$K_n = \left(\frac{2\pi m_{AB_{n-1}} m_B}{m_{AB_n}} \frac{kT}{h^2}\right)^{3/2} e^{-\Delta E_n/RT} \tag{2.6}$$

where the rotation, vibration, and electron contributions are either neglected or are assumed to cancel. The bond energies ΔE_n, which are the zero point energies, are given in Table I for SF_6 and CF_4.

The fraction of dissociation was determined by simultaneous solution of the following n equilibrium equations and the conservation equations for species A and B.

$$K_n (AB_n) = (AB_{n-1}) (B) \qquad (2.7)$$

$$K_{n-1} (AB_{n-1}) = (AB_{n-2}) (B)$$

$$\vdots \qquad \vdots$$

$$K_1 (AB) = (A) \ (B)$$

The solution to these equations was obtained, and the results for the fraction of dissociation are shown in Figure 2 and 3.

At the test conditions of 3840°K and 1 1/2 atms., calculations showed the SF_6 and CF_4 additives to be completely dissociated into atomic species (see Figures 2 and 3). This was verified by the experiments. The degree of dissociation was obtained by observing the equilibrium electron attachment existing upstream of the nozzle. The reduction in electron density with fluorine depended only on the amount of fluorine present and was independent of whether SF_6 or CF_4 was pre-mixed with the air.

The rate of dissociation of the pre-mixed additive could considerably alter the planned experiment if the rate happened to be very slow. If the dissociation rate were much slower than the ionization rate of air, then dissociation would be observed in the data as a marked decrease in the electron density from its uniform equilibrium value in air. This was not observed and equilibrium attachment effects were observed, thus the rate of dissociation of the additives SF_6 and CF_4 occurred at a faster rate than the ionization rate of air.

2.3 Electron Attachment to Fluorine

The phenomenon of electron attachment to neutral atoms and molecules has been studied for decades. The attachment of an electron to a neutral atom or molecule involves the emission of energy since the positive ion is at a lower energy level than the original neutral specie. The energy emitted in order to attach an electron is known as the electron affinity, Ea. The electron affinities of halogens are tabulated in Table II. Chlorine and fluorine atoms have the highest affinities of any known material.

The predominant atomic attachment process is a three-body collision with the third-body used to carry off the excess energy, e.g.

$$F + X + e^- \rightarrow F^- + X \qquad (2.8)$$

Electrons can attach in a two-body process with the excess energy radiated, but this is an unlikely mechanism.

The equilibrium constant for the three-body fluorine attachment reaction can be written using equation (2.3) through (2.5) and the constants in Table II.

$$K_c = \frac{1}{2} \left(\frac{2\pi m_e kT}{h^2}\right)^{-3/2} \frac{e^{-Ea/kT}}{\sum g_n e^{-\epsilon_n/kT}} \qquad (2.9)$$

The difference in zero point energy between the negative ion and the atom is the electron affinity.

The electron concentration in the presence of halogen atoms was determined from the simultaneous solution of the equilibrium equation (2.9) and the following equations for conservation atoms and charge:

$$\begin{aligned} (F) + (F^-) &= (F)_o \qquad \text{conservation of atoms} \\ (F^-) + (e^-) &= (e^-)_o \qquad \text{conservation of charge} \end{aligned} \qquad (2.10)$$

Note that $(\ )_o$ denotes initial conditions.

The solution of these equations for the electron concentration is:

$$(e) = -\left[\frac{(F)_o - (e^-)_o + \frac{1}{K}}{2}\right] + \sqrt{\left[\frac{(F)_o - (e^-)_o + \frac{1}{K}}{2}\right]^2 + \frac{(e^-)_o}{K}} \qquad (2.11)$$

The usual practice is to have the fluorine concentration much larger than the electron concentration. Under this circumstance, fluorine is not appreciably consumed and the conservation of fluorine atoms can be neglected. Then the electron concentration is given as:

$$(e^-) = \frac{(e^-)_o}{K(F)_o + 1} \qquad (2.12)$$

Electron attachment to fluorine was estimated using equation (2.12) with the results shown in Figure 4. Note that the results are presented in terms of the partial pressure of fluorine. The mole fraction of fluorine added is given by:

$$\chi = P'(F)/P$$

where $P'(F)$ is the partial pressure of fluorine, P is the air pressure, and χ is the mole fraction. The results shown in Figure 4 demonstrate that electron attachment becomes significant only when the fluorine is cooled below 3000°K. Figure 4 indicates that mole fractions of fluorine greater than 1 percent or 1/6 of one percent of SF_6 (if SF_6 completely dissociates), will cause a reduction in the electron density at the test conditions of 1 1/2 atmospheres and 3840°K. A comparison of predicted equilibrium attachment and the measured attachment, assuming complete dissociation, of SF_6 and CF_4 is shown in Figure 5. Excellent agreement was observed, confirming that complete dissociation occurred.

2.4 Experimental Techniques

A shock tube was used to produce thermal electrons in an air atmosphere having a small concentration of fluorine additives. A description of the shock tube and test instrumentation is given below.

2.4.1 Shock Tube and Nozzle

The experiments were conducted in a ten-foot long, combustion driven shock tube which exhausted into a supersonic wedge nozzle. The shock tube had an inside diameter of 1 1/2 inches with the nozzle having a 1 1/2 inch square dimension. The driven section consisted of a 1 1/2 inch pyrex tube which made possible photometric and microwave attenuation measurements at any station along the shock tube. A one-foot long square section was placed between the round pyrex tube and the nozzle throat to permit transition of the flow from a circular to square nozzle throat cross section.

The wedge nozzle was adjustable to half-angles between 0 and 15 degrees. All the current tests were conducted with the wedge at a half angle of 10 degrees. Plexiglass windows were installed in the nozzle walls along the centerline (see Figure 6) for microwave transmission.

2.4.2 Basic Wave Processes in the Shock Tube and Nozzle

The basic wave processes in the shock tube wedge nozzle are illustrated in a position-time diagram of Figure 7. This diagram shows the shock waves, the contact surface and the particle paths of several samples of air picked up by the initial shock wave at various stations along the tube.

The principal features of the flow are:

A. The initial shock wave which moves at constant speed along the constant-area tube and then slows down in the nozzle.

B. The upstream-facing "starting shock" in the nozzle which is swept downstream by the flow. This is analogous to the starting shock in an ordinary wind-tunnel nozzle.

C. The constant surface between the driver and driven gases. This moves at a constant speed along the constant-area tube and then accelerates in the nozzle.

D. The shock wave driven ahead of the accelerating contact surface.

Samples of air picked up at different points along the shock tube are subjected to radically different thermodynamic processes, as indicated by the pertinent particle paths. An instrument examining the air passing by a fixed location in the nozzle sees first the region between the two shocks A and B. In this region the conditions are not constant. Initially the instrument sees air which has been compressed by the initial shock but not expanded. Somewhat later the air passing the instrument has been compressed in the constant area tube, expanded in the nozzle and compressed again by the starting shock.

Next the instrument views the region between B and D. There, conditions are uniform, all this air having been compressed in the constant-area section and then expanded through the same area-ratio in the nozzle. This constitute the desired test sample.

Finally the instrument views the air in the region between C and D, which has been processed initially in the same manner as the test sample, but then has been overtaken by the shockwave D.

The shock speed was determined by detecting the passage of the shock wave at two shock tube positions using phototubes. Phototubes were also used to observe uniformity of the test region by measuring the intensity of the air radiation.

Measurements of shock wave attenuation and test time were made at various stations along the shock tube. Beyond 12 feet, the shock wave attenuated at a rate of 0.07 mm/μs/ft. No noticeable attenuation was observed between 5 and 12 feet. As a result of these measurements, the

shock tube was shortened to 10 feet to minimize any shock attenuation. The observed test time in the shock tube averaged 120 μs for shock speeds of 3.7 mm/μs at initial pressures of 7.6 mm Hg. This is half way between the turbulent and laminar values for test time given by Mirel (Reference 2). The test time was reduced in the nozzle to between 60 and 70 μs.

2.4.3 Microwave Diagnostics

A 24 kmc microwave interferometer was used to measure the electron density and collision frequency of the ionized air. The interferometer, shown schematically in Figure 8, employed four probes. The transmitted and reference signals were resolved into phase shift and attenuation signals as described in detail in Appendix B. The measured phase shift and attenuation were interpreted using the theory of microwave propagation through a bounded plasma developed by Bachynski (Reference 3) and described in Appendix C. For the 1 1/2 inch plasma slab and the two 1/2 inch plexiglass windows, the relation of density and collision frequency to phase shift and attenuation is shown in the map in Figure 9. The plasma frequency and collision frequency were normalized with respect to the propagation frequency, i. e.,

$$S = \nu/\omega$$

$$N = (\omega_P/\omega)^2$$

where:

S	normalized collision frequency
ν	collision frequency
N	normalized plasma frequency
ω_P	plasma frequency
ω	microwave frequency

The microwave interferometer was calibrated periodically using a calibrated phaseless attenuator and a phase shifter. Figure 10 shows the calibration at all phases. Prior to each run, the 48 db signal level was recorded at 0° phase angle (see Figure 11).

2.4.4 Addition of Electrophilic Gases

The electrophilic gases were pre-mixed with the air in the driven section of the shock tube. The experiments were conducted with electrophilic gases added in concentrations ranging between 0.03 to 3 percent by volume.

The test plan was to hold the initial driven pressure fixed at 0.01 atm and to maintain a constant shock speed at 3.7 mm/μs. Earlier shock tube runs showed that the pre-mixing of the driven air with the additives slowed down the shock speed. This effect was not attributed to the change in the mixture molecular weight or ratio of specific heats, but was due to the real gas effects occurring from the dissociation of the electrophilic additives. A detailed examination of this effect by calculation of a real gas shock wave for the specified mixture was not attempted at this time. The decrease in shock speed was remedied by altering the composition of the combustion driver gases (70 percent H_e, 20 percent H_2, 10 percent O_2). Dry nitrogen was added to the combustion gas to reduce the shock strength produced. It was then a simple matter to maintain a constant shock speed by decreasing the amount of nitrogen added to the driver as the electrophilic additive was added to the driven air.

3.0 EXPERIMENTAL RESULTS

Numerous shock tube runs were made comparing the electron density with and without fluorine gas in the air. A few runs were made with $CC\ell_4$ and water vapor pre-mixed with the air. However, insufficient data was obtained to compare attachment to chlorine or water vapor with fluorine electron attachment.

During the contract period, a total of 152 data runs were obtained in the following categories:

Gas Additives	No. of Data Runs
Freon-14 (CF_4)	45
SF_6	43
$CC\ell_4$	10
Water Vapor	9
Air	45

Microwave interferometer measurements were made at stations -3, 10, 15, and 20 inches downstream from the nozzle throat. At each station, the electron density and collision frequency were measured as a function of laboratory time.

Representative test results are shown in Figure 11. The measurements are shown in functions of laboratory time at a particular nozzle station. The observer first views the particles that have had only a short residence time behind the shock wave and have not achieved equilibrium conditions. At a later time the particles have had a sufficient residence time to achieve equilibrium and a uniform level of ionization is measured. The uniform equilibrium conditions persist until the contact surface arrives. For each run, the attenuation and phase were obtained using equations B-5 and B-6. Then in turn, the plasma frequency and collision frequency were obtained by inverting the analysis described in Appendix C by the use of Figure 9.

3.1 Collision Frequency

The measured collision frequency of the ionized air is shown in Figure 12. The measurements upstream of the nozzle are about one-third the calculated values of Bachynski (Reference 4), Musal (Reference 5) and Friel (Reference 6) as is illustrated below:

Collision Frequency	Reference	Equation
3×10^{10}	This Report	
9×10^{10}	Musal	$1.5 \times 10^{10} \sqrt{T p}$
1.5×10^{11}	Bachynski	
2.34×10^{11}	Friel	$1 \times 10^{13} \frac{P}{\sqrt{T}}$

The addition to the air of fluorine and other additives did not change the measured collision frequency.

3.2 Density in the Nozzle

The mass density in the nozzle was not explicitly measured, but was inferred from the collision frequency measurements. The decrease in the collision frequency down the nozzle was attributed to the density expansion. This measured density expansion was found to match the area expansion for an ideal 4 degree wedge nozzle. Thus, though the actual nozzle angle was set at 10 degrees, the flow is analyzed on the basis of a frozen 4-degree expansion. Non-ideal expansion would be expected to occur from the boundary layer displacement. Note also that the expansion was observed to begin about four inches downstream of the nozzle entrance; a consequency of the small Mach angle of the flow.

The measured electron densities in the shock tube agreed with expected equilibrium values (Reference 7). The measured values of electron density down the nozzle are given in Figures 13 and 14. The measurements clearly demonstrate the reduction of electron density when fluorine is added.

4.0 DATA ANALYSIS

The experimental measurements of the decay in the electron density down the nozzle are now analyzed to obtain the three-body reaction rate coefficient. The analysis attributes the time rate of change of the electron density observed with fluorine, over and above the changes without fluorine, to be the attachment rate. The method of analysis is described in the following discussion.

The measurements at the individual nozzle stations were transformed from laboratory coordinates to Lagrangian coordinates. The time for a particle to flow from the nozzle throat to the viewing station is given as:

$$t = \int_{o}^{\ell} \frac{dx}{U} \tag{4.1}$$

where U is the flow velocity, ℓ the distance between the throat and the viewing station, and t is the Lagrangian time.

The attachment rate was determined from measurements with and without the additives present. The difference in the rate-of-change of electron density with and without the additives was identified with the attachment rate, e. g.:

$$\frac{-d\left[(e^-) - (e^-)_n\right]}{dt} = k_a (e^-) (F) (X) \tag{4.2}$$

where $(e^-)_n$ represents the electron density without additives and (e^-) represents the electron density with additives. For small intervals of time where the temperature and density decrements are a small percentage of the initial values, the rate constant could be evaluated

from the experimental data using the following equation:

$$k_a = \frac{\Delta e_{t2} - \Delta e_{t1}}{(e^-)(F)(X)(t_2 - t_1)} \qquad (4.3)$$

where $\Delta e_{t1} = (e^-)_{nt_1} - (e^-)_{t_1}$ and $(e^-) = \left[(e^-)_{t_1} + (e^-)_{t_2}\right]/2$ and t represents time at stations 1 and 2. The experimental measurements however, were not made at close enough intervals to justify the assumption of a constant rate coefficient. Therefore, it was necessary to assume a temperature dependence for the rate coefficient and then evaluate equation (4.2).

The rate coefficient was assumed to have the Arrhenius form (Reference 8)

$$k_a = A\, e^{-E/RT} \qquad (4.4)$$

where A is the frequency factor and has the same units as k_a, which are taken to be cc^2 molecules^{-2} s^{-1}. E is the Arrhenius activation energy in calories per mole. Since the negative ion does not exist in an excited state the activation energy should be equal to, or greater than the electron affinity. The frequency factor A was evaluated from the following equation using the Arrhenius rate coefficient (Equation 4.4).

$$A = \frac{\Delta e_{t2} - \Delta e_{t1}}{\int_{t1}^{t2} (e^-)(F)(X)\, e^{E/RT}\, dt} \qquad (4.5)$$

The procedure for determining the rate coefficient was to find the value for the activation energy, E, which would give a constant frequency factor. Equation (4.5) was fitted to the data in Figure 15 assuming values for E of 60, 84, 96 and 100 kcal/mole. A constant frequency factor was obtained for an activation energy of 84 kcal/mole which is the attachment energy. Thus the attachment rate coefficient was determined as:

$$k_a = 1.5 \times 10^{-37}\, e^{(84,000 \pm 4,000)/RT}\ cc^2\text{-molecules}^{-2}\text{-s}^{-1} \qquad (4.6)$$

5.0 CONCLUSIONS

A shock tube technique was developed to obtain the three-body electron attachment rate coefficient for fluorine. The shock tube simulated re-entry plasmas of one atm pressure with about 10^{13} electrons/cc density.

The SF_6 and CF_4 that were pre-mixed with the air in the shock tube completely dissociated prior to the ionization of the air. Excellent agreement was obtained between the calculated and the measured equilibrium electron density in the shock tube when electron attachment to dissociated fluorine atoms was assumed.

The electron attachment to atomic fluorine was measured as the shock tube flow expanded through a hypersonic wedge nozzle. The difference in the measured electron densities with and without the fluorine was analyzed in terms of a rate coefficient. The rate coefficient determined was

$$k_a = 1.5 \times 10^{-37} e^{(84,000 \pm 4,000)/RT} \text{ cc}^2 \text{ - molecules}^{-2} \text{ -s}^{-1}$$

The activation energy determined from experiments had the same value as the electron affinity of fluorine.

These measurements demonstrate the two attractive features that can be gained by injecting SF_6 or CF_4 into a high pressure re-entry plasma. The SF_6 and CF_4 can dissociate to cool a hot plasma leaving atomic fluorine. The atomic fluorine can attach electrons to alleviate high pressure plasma blackout.

TABLE I

Specie	Molecular Weight g/mole M	Specific Heat cal/mole-°c C_P	Enthalpy at 300°K cal/mole H_{300}	Bond Energy kcal/mole ΔE	ΔH Dissociation kcal/mole
SF_6	146.06	23.22	6945	85	426
SF_5	127.06	4R	----	65	---
SF_4	108.06	4R	----	65	---
SF_3	89.06	4R	----	65	---
SF_2	70.06	4R	----	65	---
SF	51.06	7/2R	----	65	---
S	32.06	5.66	----	--	---
F	19	5.436	----	--	---
CF_4	88.01	4R	5992	123	462
CF_3	69.01	4R	----	113	---
CF_2	50.01	4R	----	113	---
CF	31.01	7/2	----	113	---
C	12.01	4.98	----	--	---

TABLE II

Properties of Halogen Gases

Species	Ionization Energy ev	Electron Affinity kcal/mole	Energy Level n	Electronic Degeneracy g_n	Electronic Energy ϵ_n, ev
F	17.418	-83.7	0	4	0
			1	2	12.71
Cℓ	13.01	-87.2	0	4	0
			1	2	0.109
			2	1	8.825
Br	11.84	-81.6	0	4	0
I	10.454	-74.7	0	4	0

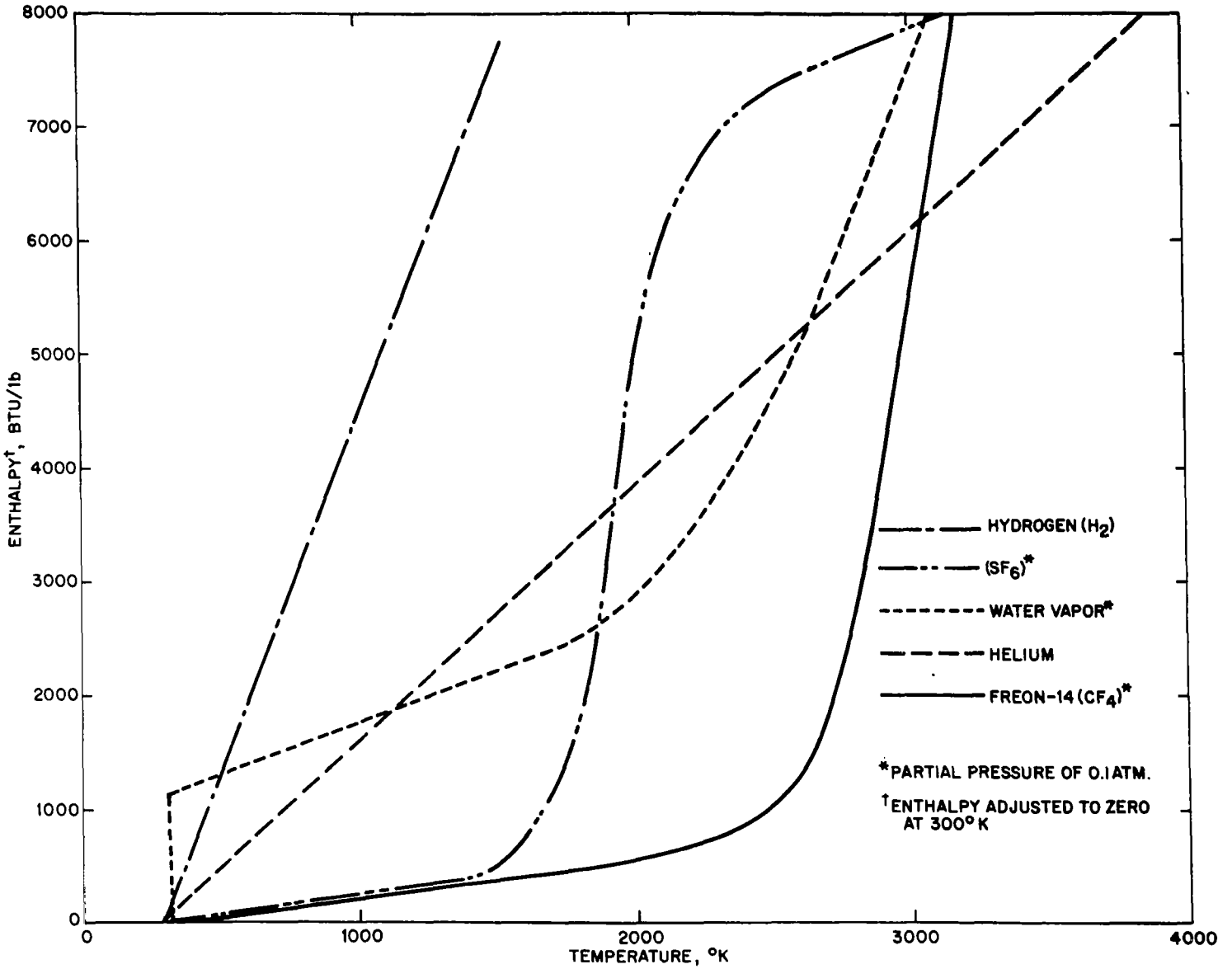

Figure 1. Comparison of the enthalpy of coolants.

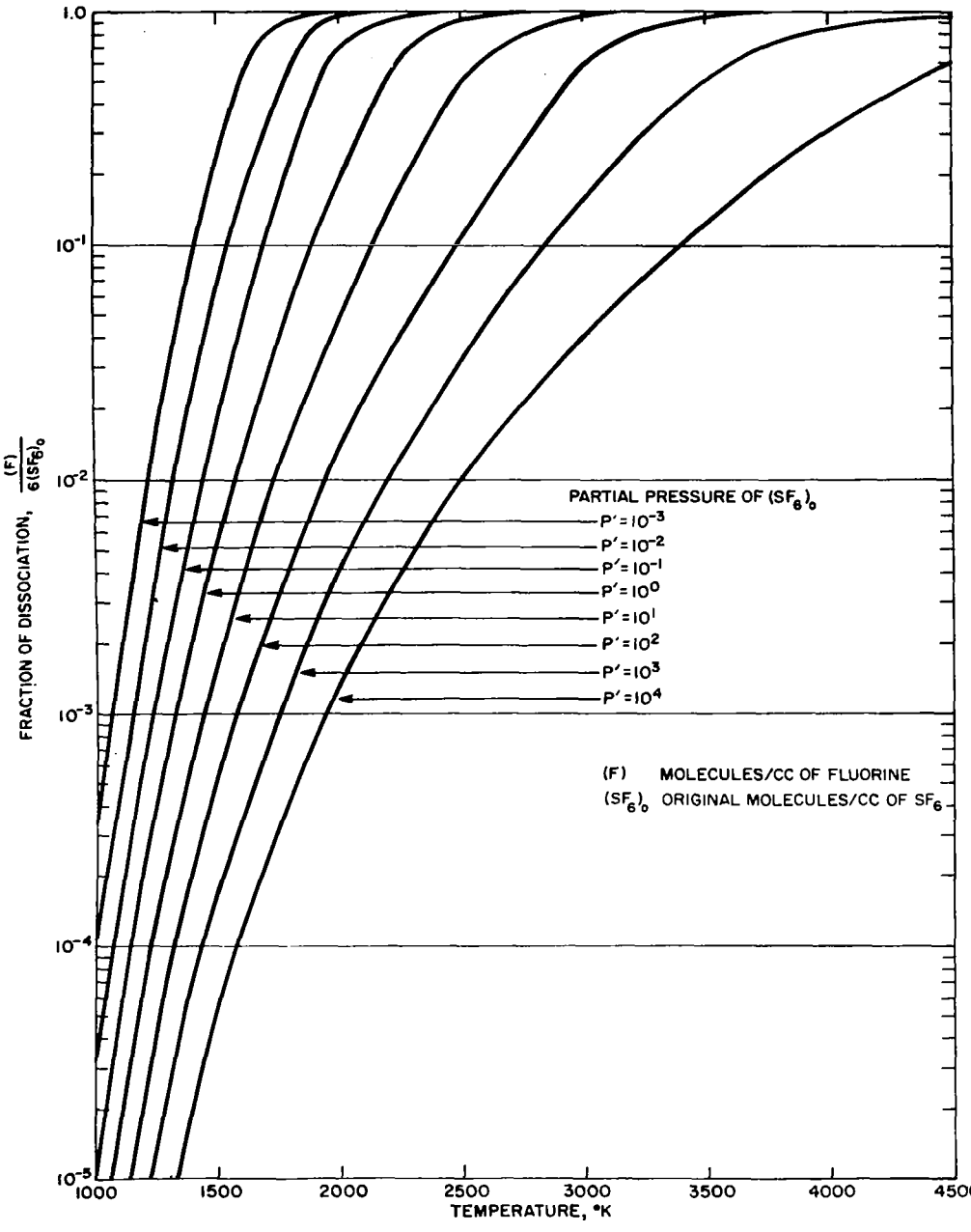

Figure 2. Fraction of dissociation of SF_6.

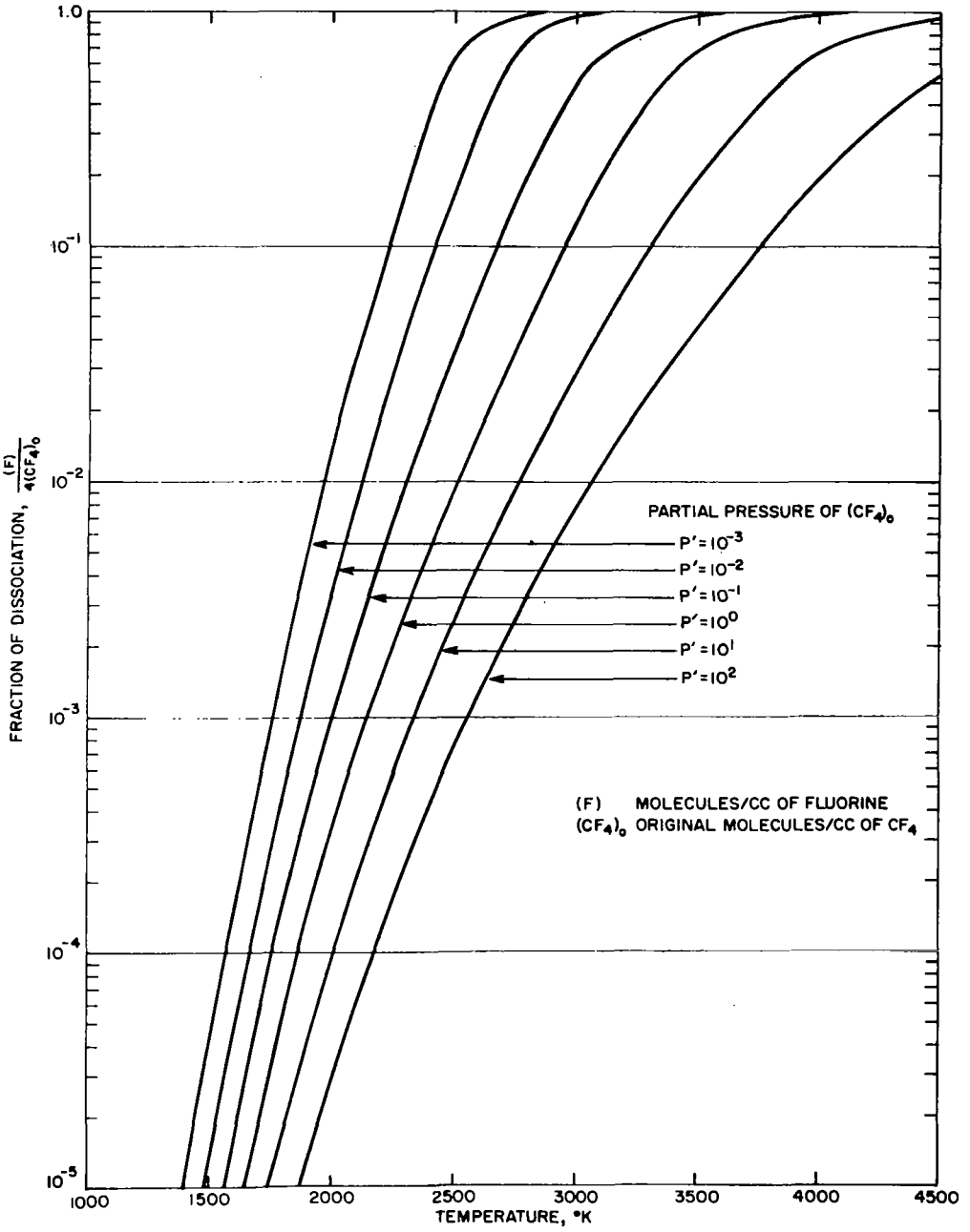

Figure 3. Fraction of dissociation of CF_4

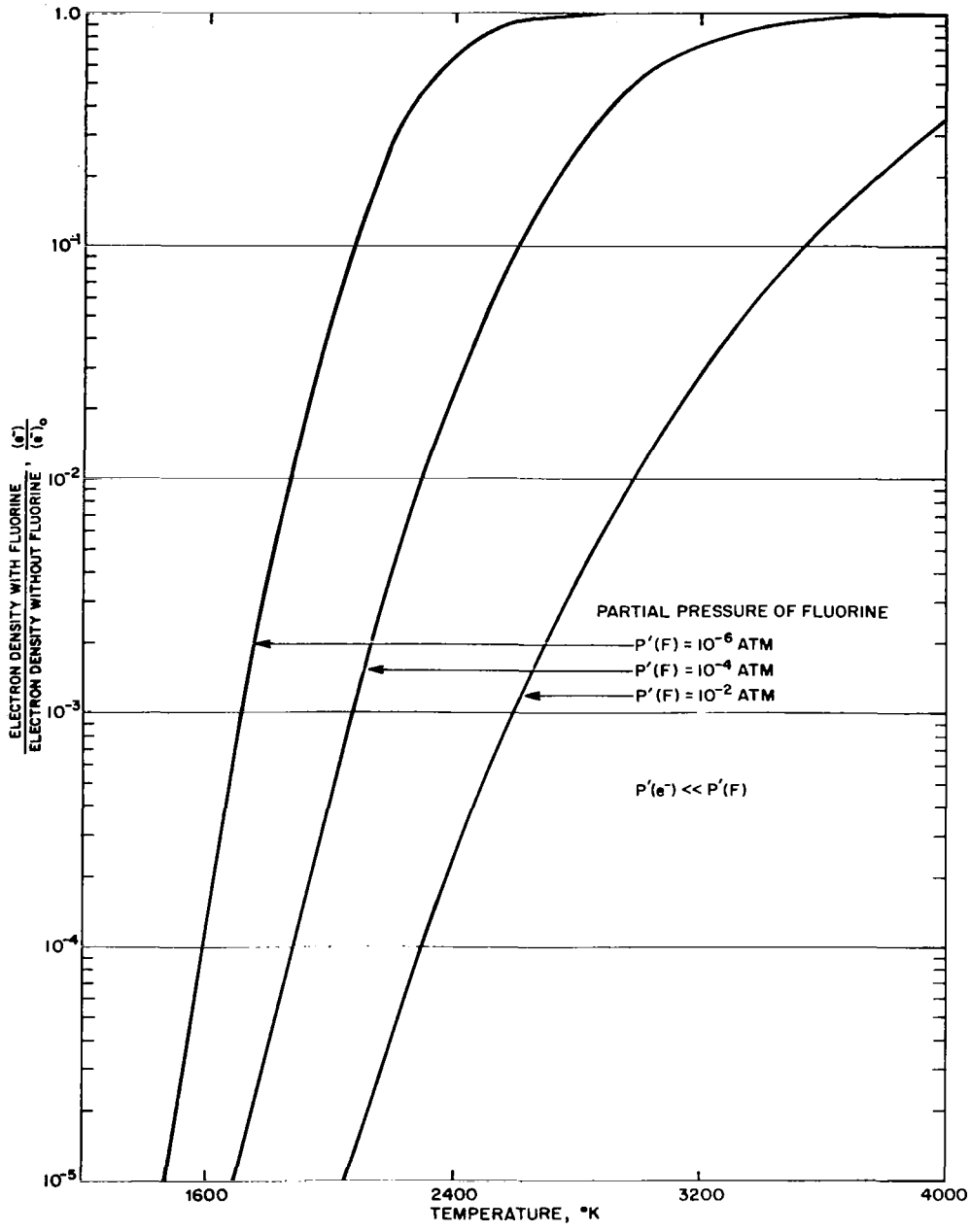

Figure 4. Electron density with fluorine attachment.

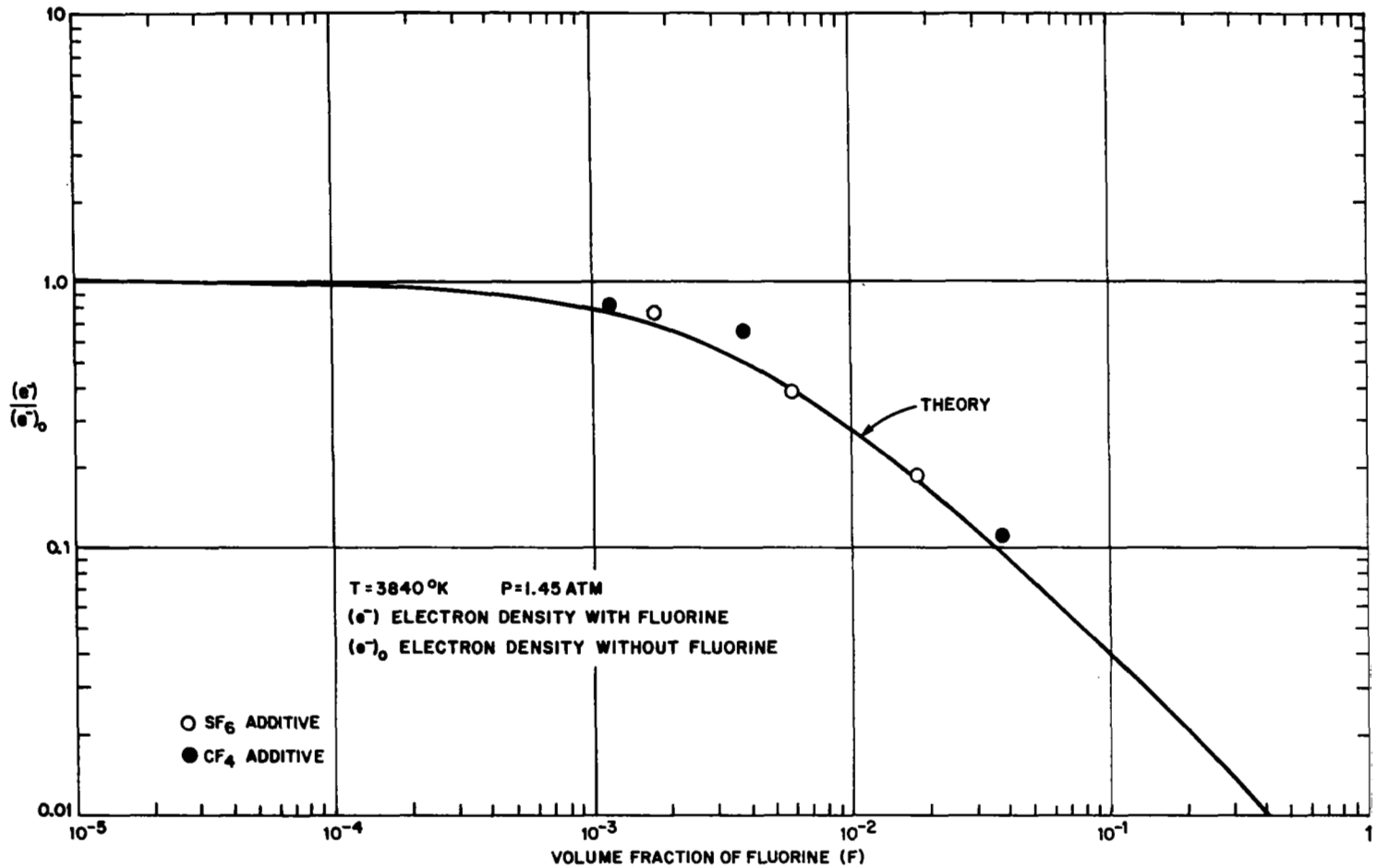

Figure 5. Electron density with equilibrium attachment to fluorine.

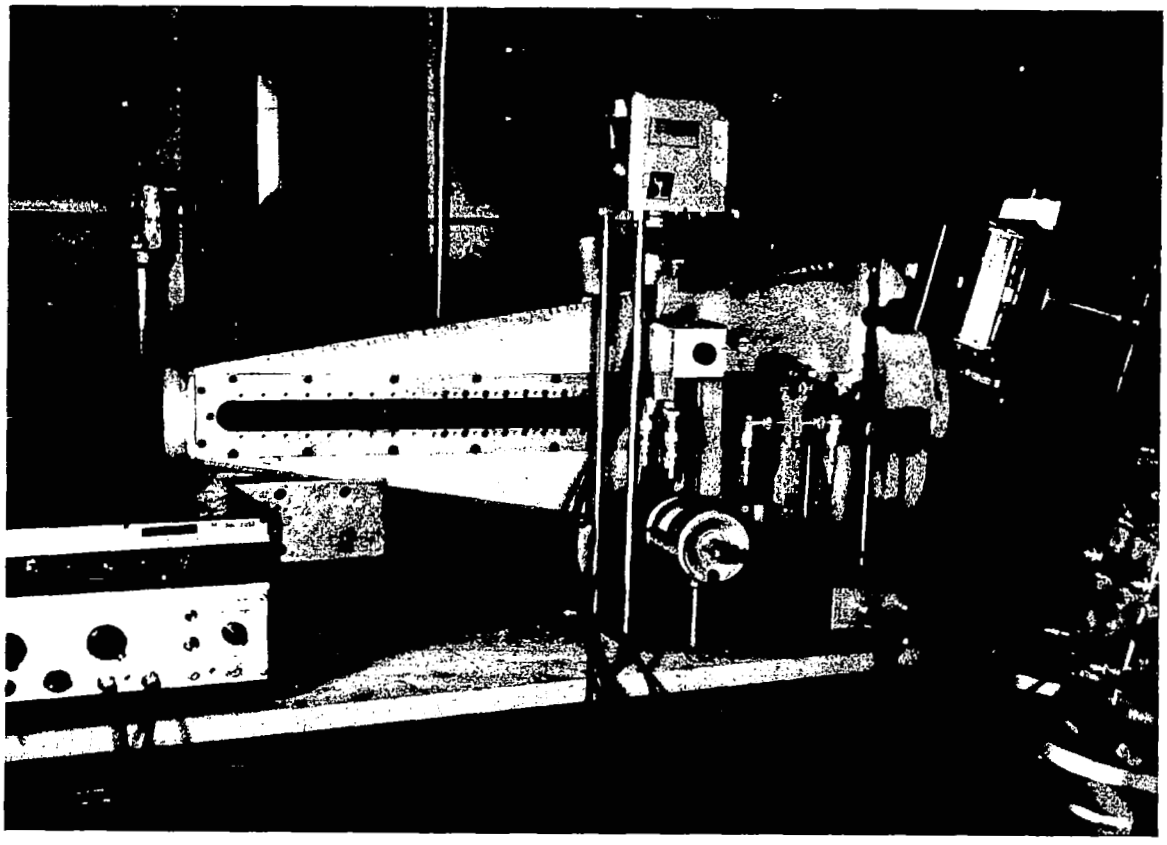

Figure 6. Shock tube.

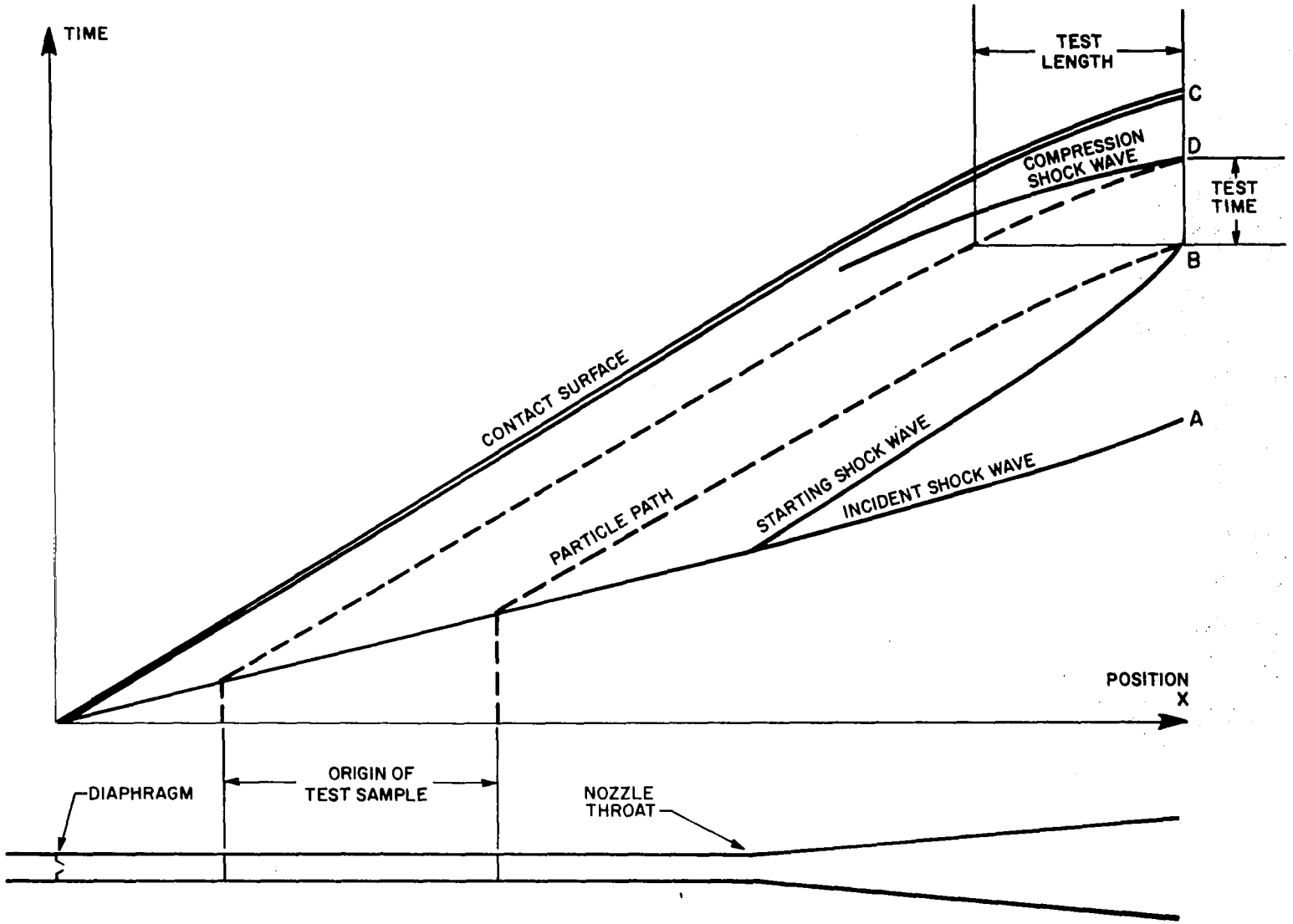

Figure 7. Position-time diagram for shock tube.

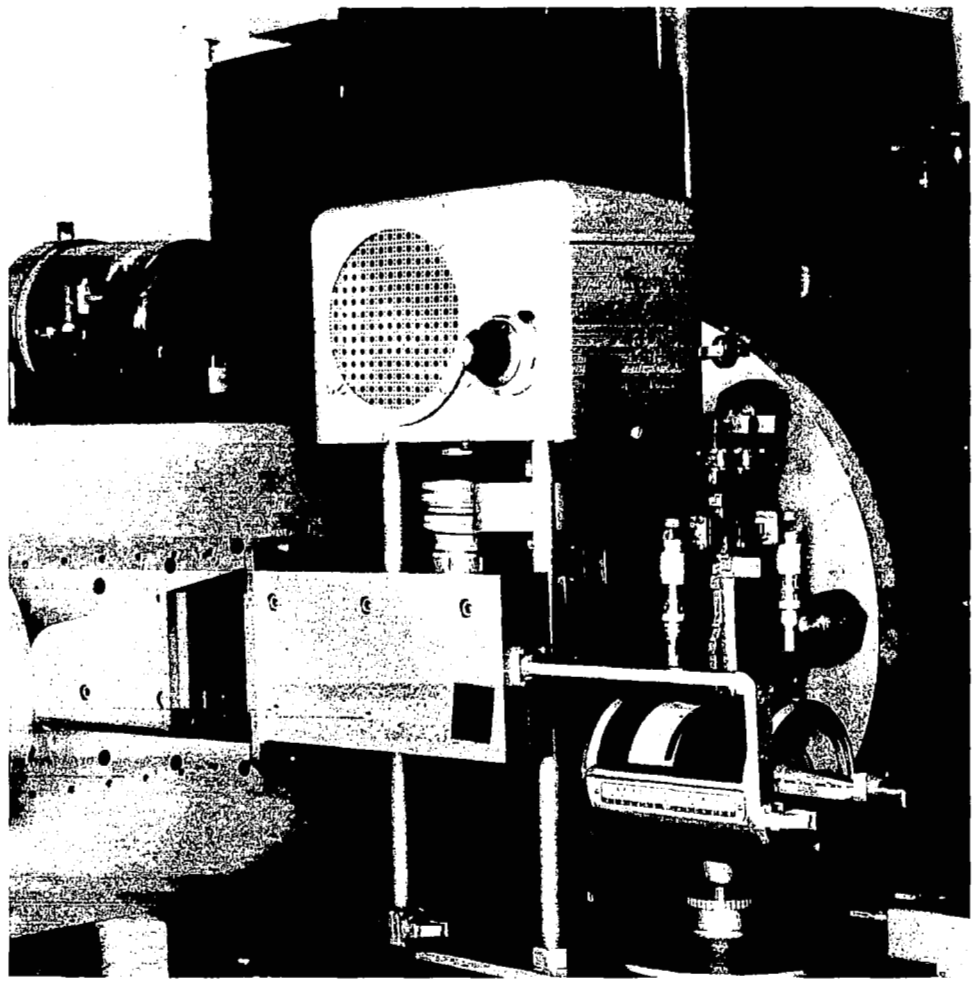

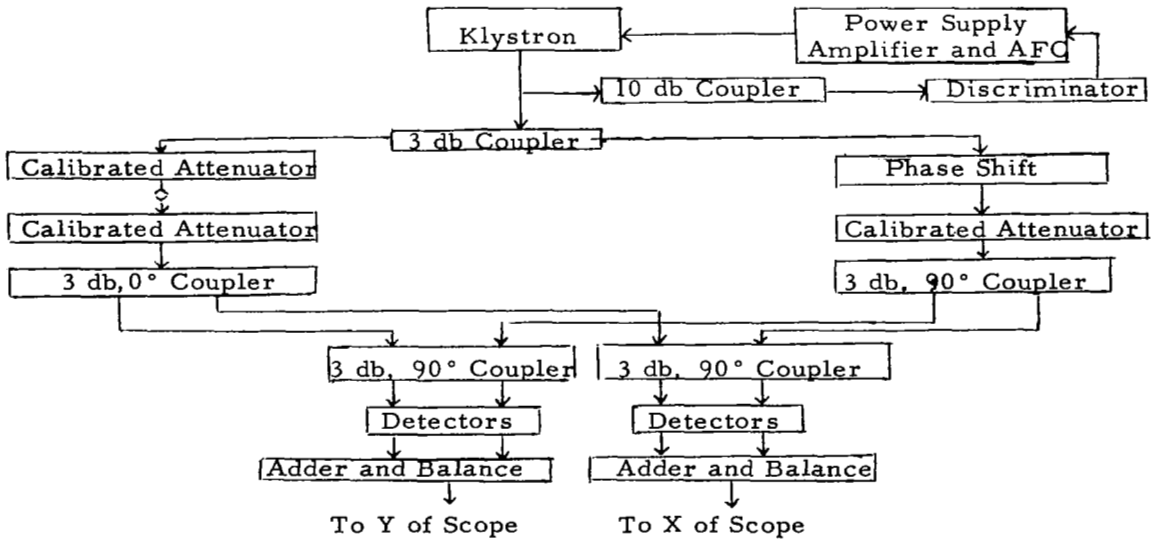

Figure 8. Schematic of microwave interferometer.

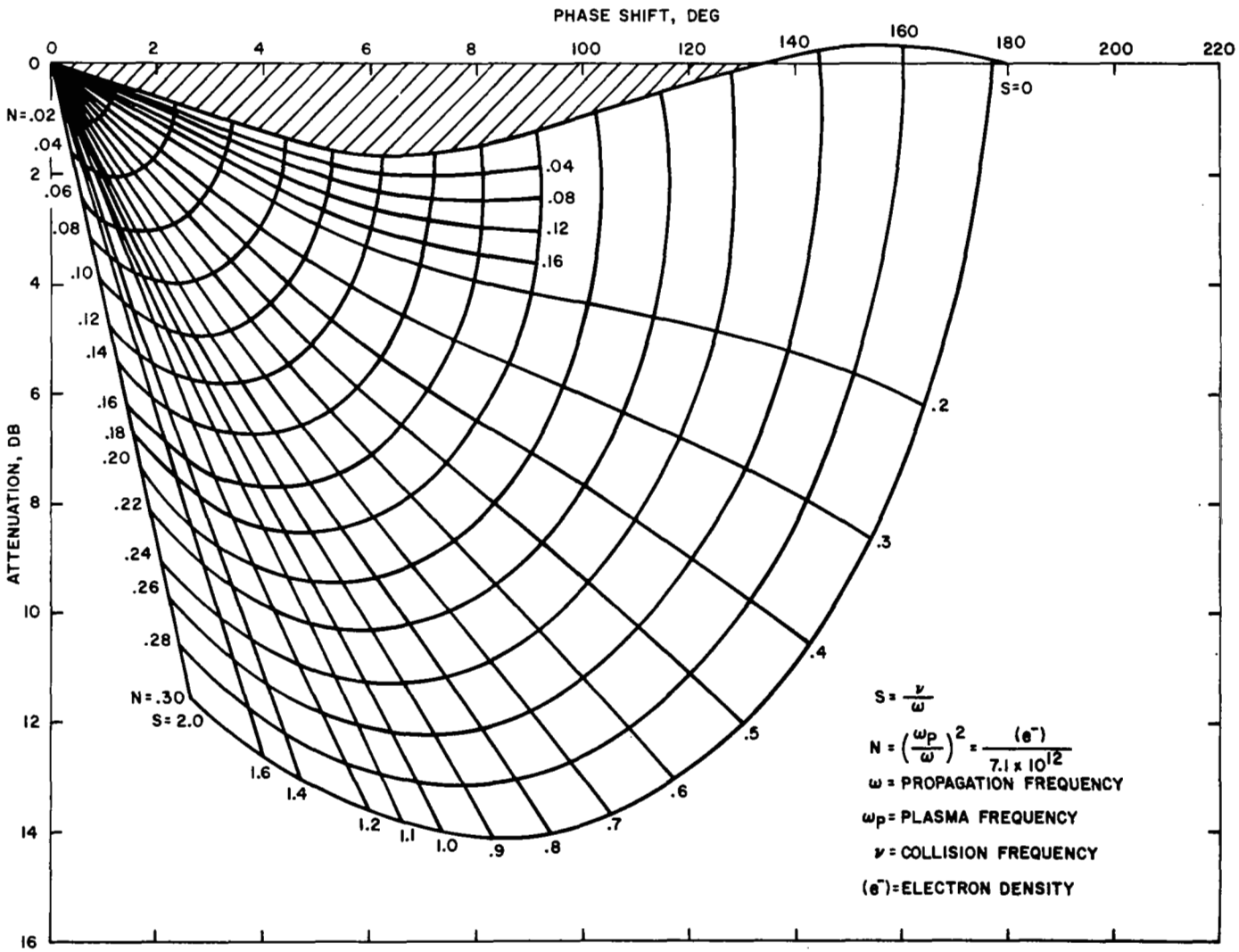

Figure 9. Normalized plasma and collision frequency versus MW attenuation and phase shift.

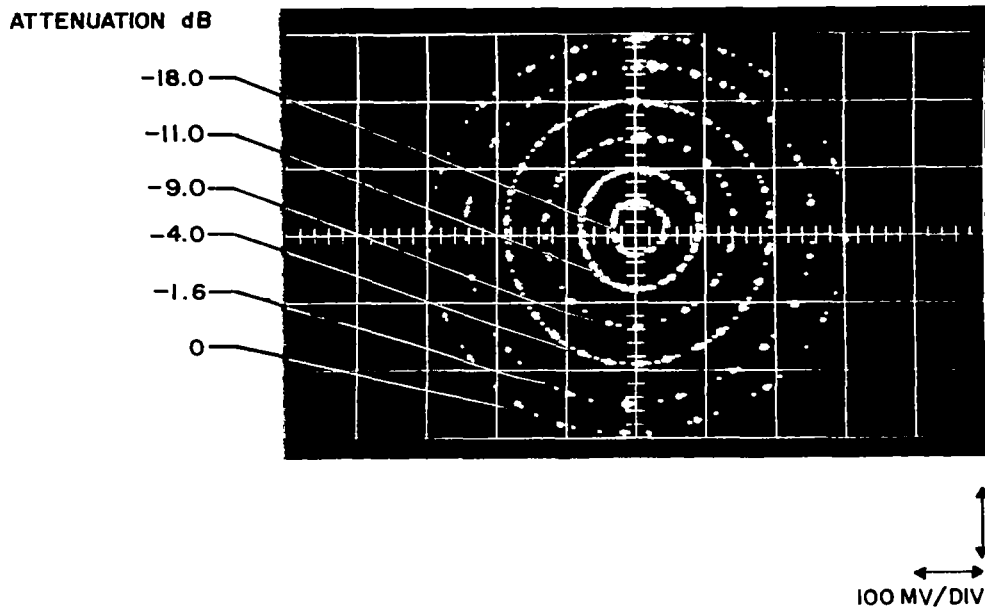

Figure 10. Microwave calibration.

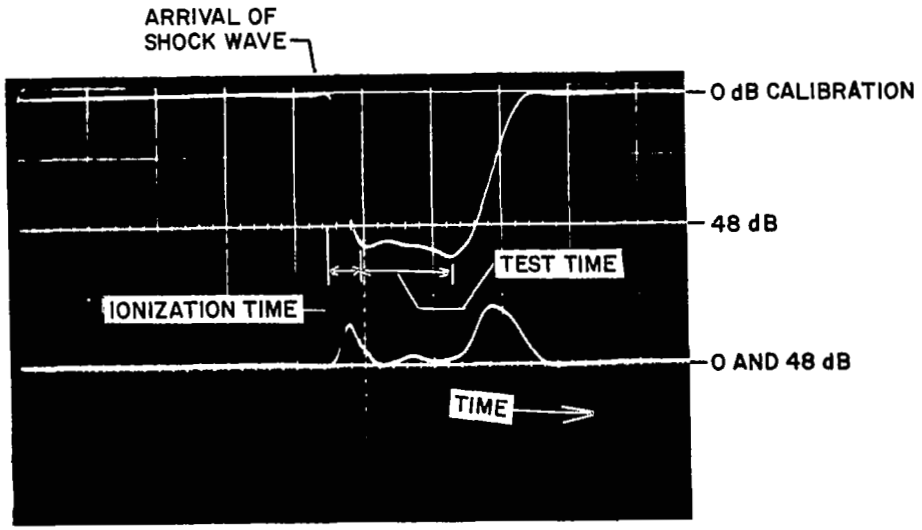

RUN NO. 441
U_s = 3.62 MM/μS
AIR ONLY

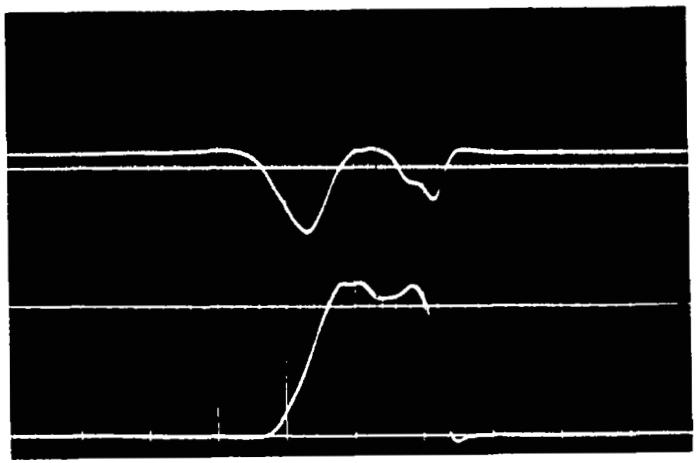

RUN NO. 398
U_s = 3.77 MM/μS
CF_4 = 0.1 %

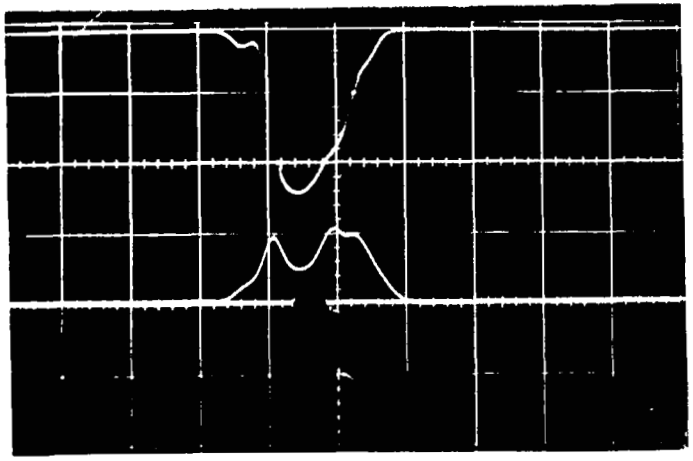

RUN NO. 487
U_s = 3.7 MM/μS
SF_6 = 0.03 %

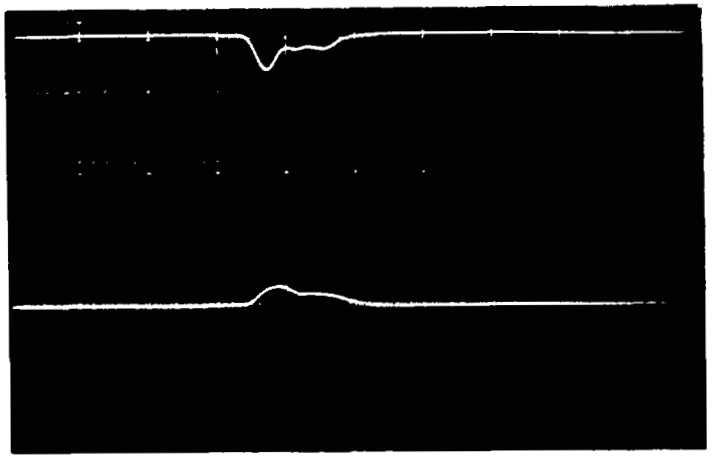

RUN NO. 444
U_s = 3.82 MM/μS
SF_6 = 0.3 %

Figure 11. Representative microwave measurements.

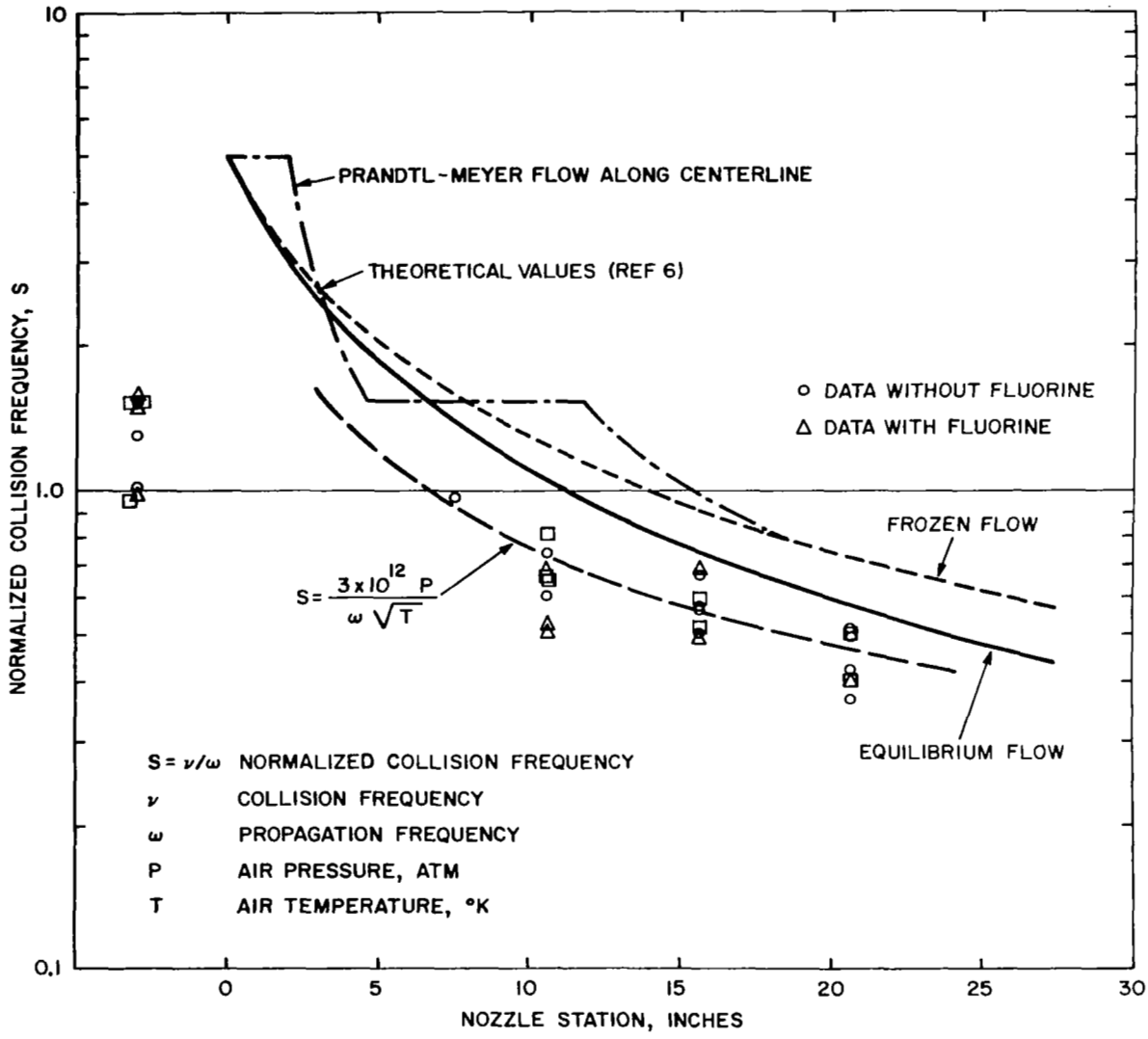

Figure 12. Normalized collision frequency of air.

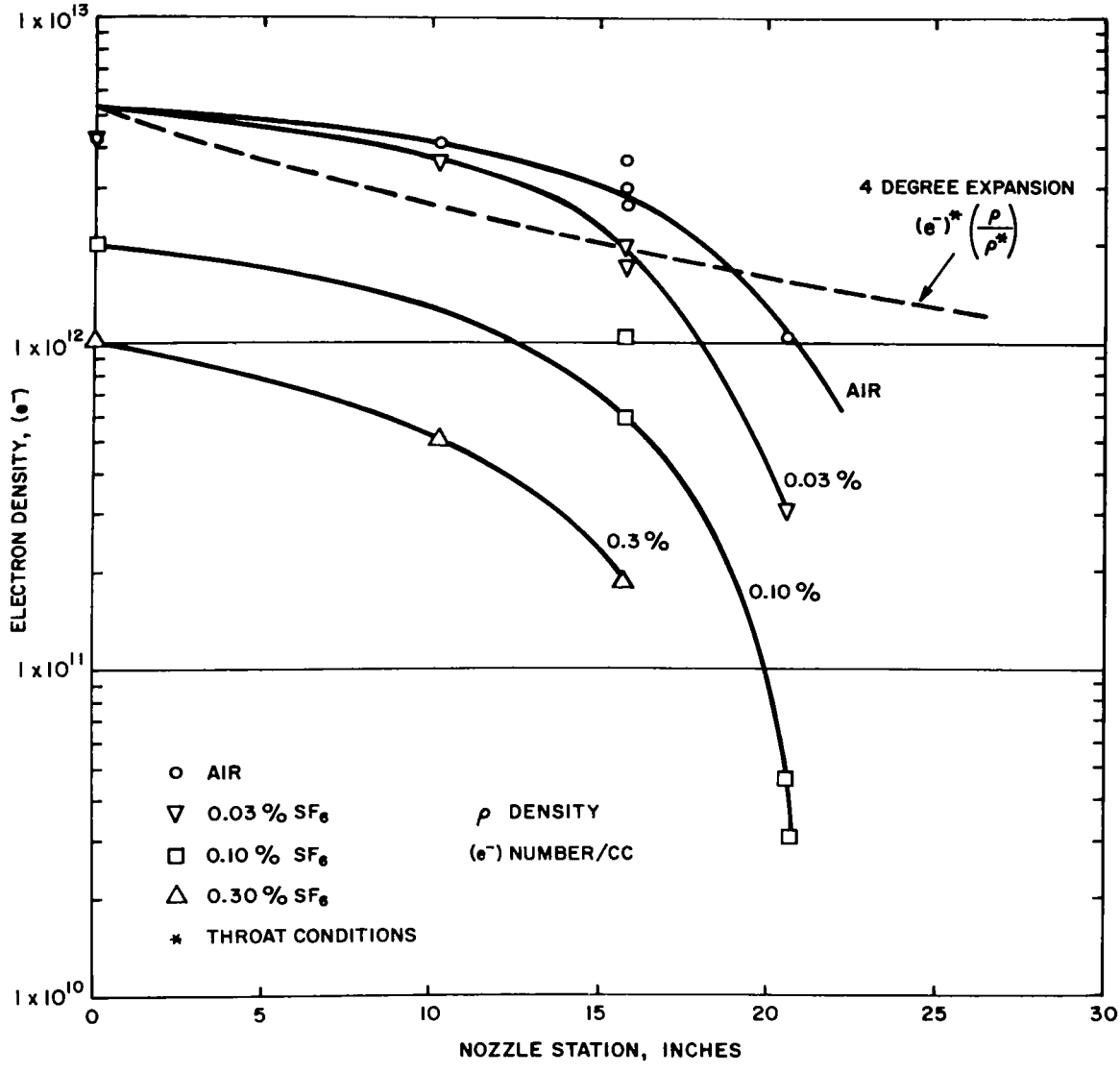

Figure 13. Electron density with SF_6 additive.

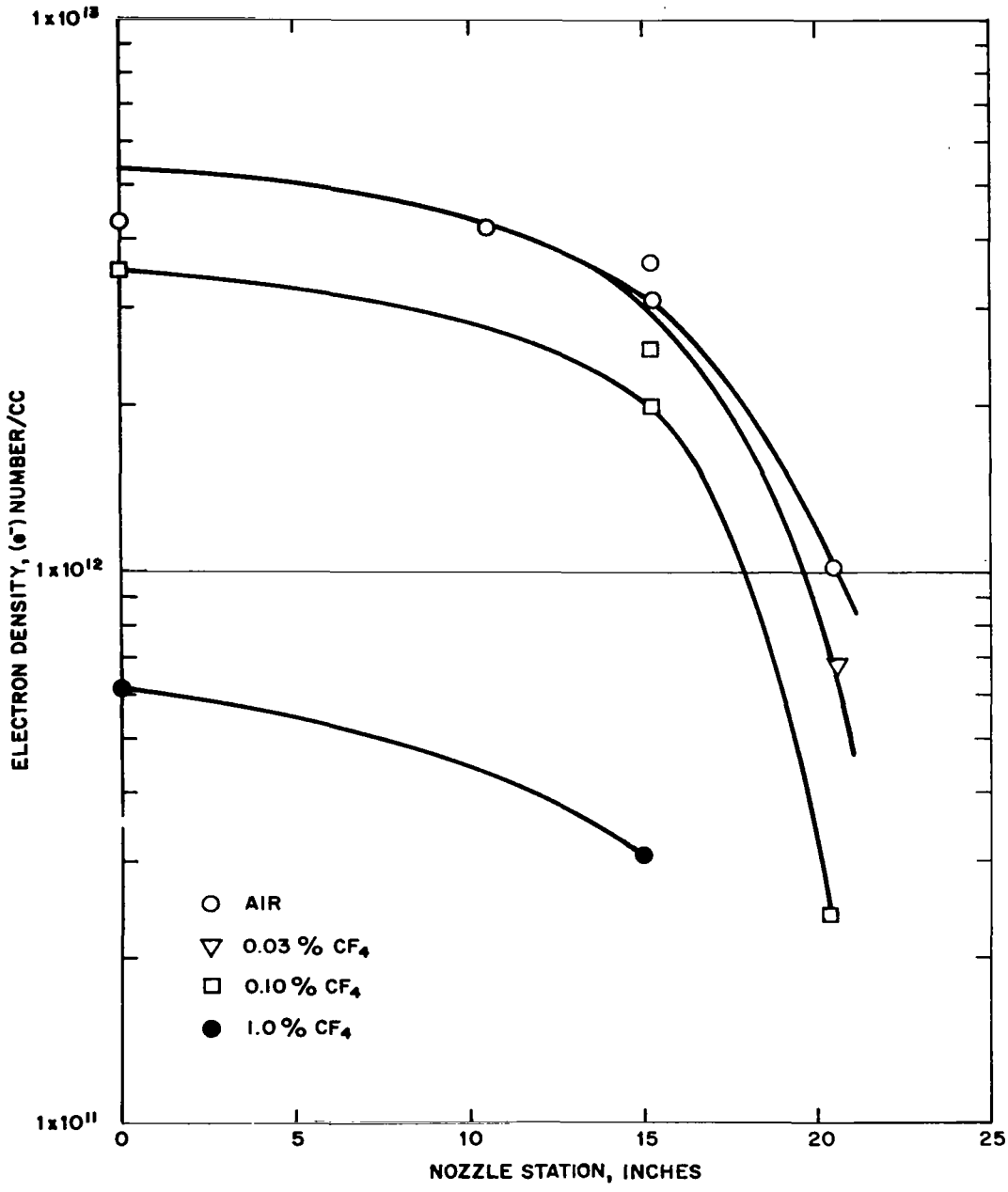

Figure 14. Electron density with Freon-14 (CF_4) additive.

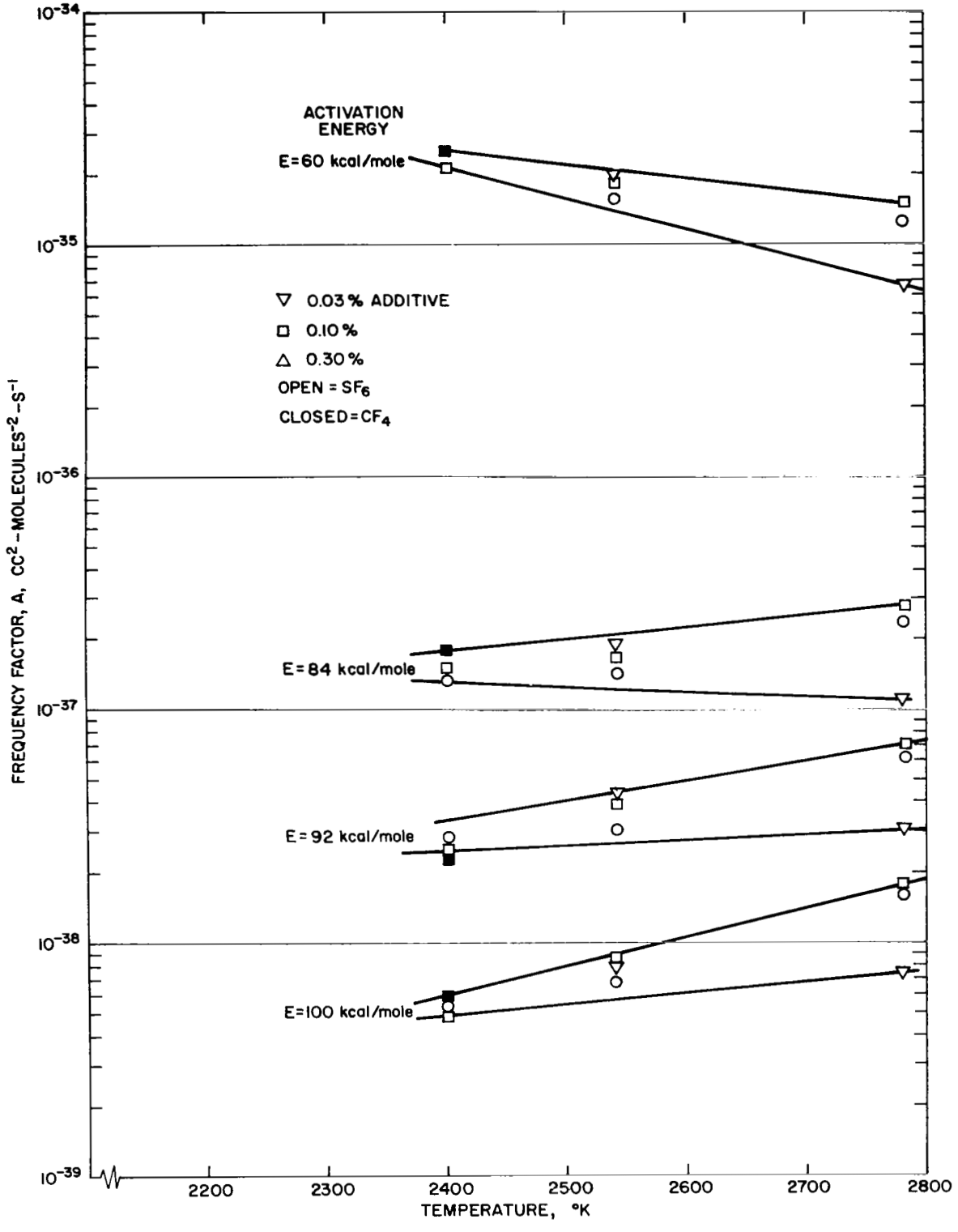

Figure 15. Experimental frequency factor.

APPENDIX A

List of Symbols

A	frequency factor
A_i	atom or molecule of species i
E_a	electron affinity
E_o	zero-point energy
E_n	bond energy
(e^-)	electron number concentration
(F)	fluorine number concentration
g_n	electron degeneracy
K_c	equilibrium constant
h	Planck constant
k_a	attachment rate constant
k	Boltzmann constant
m	mass
N	normalized plasma frequency
P'	partial pressure
P	pressure
$Q(A_i)$	partition function
R	universal gas constant
S	normalized collision frequency
t	time
T	temperature
U	velocity

x	position
(X)	third body number concentration
ϵ_n	electron excitation level
χ	mole fraction
$(\ )_o$	original concentration, molecules/cc
ν	collision frequency
ω	propagation frequency
ω_P	plasma frequency

Subscript

o	initial condition
1	first nozzle station
2	second nozzle station
n	without additives

APPENDIX B

Measurement of Transmitted Microwave Power and Phase

The measurement of the plasma frequency and collision frequency was accomplished using a Strand Labs microwave interferometer. The interferometer consisted of four probe detectors which measured the reference and transmitted power and phase. The interferometer was operated at 24 kmc with an EMI R9602 klystron using the TE_{011} mode at a maximum voltage level of 200 mv. The signal was transmitted through a collimating lens, two 1/2-inch plexiglass windows and a 1 1/2 inch-wide plasma, into a collecting lens.

The four probes measure the vector sum of the reference signal (Vr) and transmitted signal (Vs) at various phase angles. The vector sum was determined using the cosine law:

Detector Probe	Signals	Sum
1	$Vr\ (\theta r) + Vs\ (\theta s)$	$(Vr^2 + Vs^2 + 2Vr\ Vs \cos\theta)^{1/2}$
2	$Vr\ (\theta r + 90) + Vs\ (\theta s)$	$(Vr^2 + Vs^2 + 2Vr\ Vs \sin\theta)^{1/2}$
3	$Vr\ (\theta r) + Vs\ (\theta s + 90)$	$(Vr^2 + vs^2 - 2Vr\ Vs \sin\theta)^{1/2}$
4	$Vr\ (\theta r + 90) + Vs(\theta s + 90)$	$(Vr^2 + Vs^2 - 2Vr\ Vs \cos\theta)^{1/2}$

(B. 1)

The interferometer was operated with the transmitted signal 1/10 of the reference signal. At this condition, Equations (B. 1) were approximated by a truncated series. The signal at detectors 1 and 4 would be

$$V_1 = Vr\left(1 + \frac{Vs}{Vr}\cos\theta + \frac{Vs^2}{2Vr^2}\right)$$

$$V_4 = Vr\left(1 - \frac{Vs}{Vr}\cos\theta + \frac{Vs^2}{2Vr^2}\right) \qquad \text{(B.2)}$$

For a crystal having a dc output voltage which is some general function of the rf voltage,

$$V_{DC} = f(V_{rf}),$$

the change in the dc voltage due to the change in the peak rf voltage may be written as a Taylor series expansion of f(V):

$$V = V_o + V, \qquad V \ll V_o$$

$$V_{DC} = f(V_o) + \frac{\partial f}{\partial V}\bigg|_{V_o} V + \frac{1}{2}\frac{\partial^2 f}{\partial V^2}\bigg|_{V_o} V^2 + \ldots$$

For functions of f(V) that one can expect to find in detectors, the first derivative exists, and the product of this derivative with a small voltage change is the predominant term. On this basis, the output from Crystal No. 1 and No. 4 may be written as:

$$V_{1,\,4} = f(Vr) \pm \frac{\partial r}{\partial V}\bigg|_{Vr}\left(Vs\cos\theta \pm \frac{Vs^2}{Vr}\right)$$

with the higher order terms suppressed as being unimportant because of the large Vr/Vs ratio. The two crystal outputs are initially balanced with a potentiometer, so the difference between the two crystal outputs is linear.

$$Vout = V_1 - V_4 = Vs\cos\theta\left[\frac{\partial f_1}{\partial V}\bigg|\, Vr_1 + \frac{\partial f_2}{\partial V}\bigg|\, Vr_2\right] \qquad \text{(B.3)}$$

If the reference signal voltage is kept constant in amplitude, the derivative terms will be constant; thus we can simplify equation (B.3) by writing it in terms of a constant:

$$V_{out\ 1,\ 4} = \alpha V_s \cos\theta \qquad (B.4)$$

The identical operations are performed with detectors 2 and 3 to yield:

$$V_{out\ 2,\ 3} = \alpha Vs \sin\theta$$

These two resultant signal voltages are recorded on an oscilloscope as a function of time.

The actual measurements were conducted with the phase initially at zero. Thus the initial voltages are:

$$V_{out\ 2,\ 3} = 0$$

$$V_{out\ 1,\ 4} = \alpha Vs$$

A typical oscilloscope trace is shown in Figure 11. The desired measurement of transmitted signal and phase was determined as:

$$\alpha Vs = \sqrt{V_{1,\ 4}^{2} + V_{2,\ 3}^{2}}$$

The phase is given by:

$$\theta = \tan^{-1}\left(\frac{V_{out\ 2,\ 3}}{V_{out\ 1,\ 4}}\right) \qquad (B.5)$$

The attenuation is defined as:

$$A = 20 \log_{10} \frac{(\alpha Vs) \text{ without plasma}}{(\alpha Vs) \text{ with plasma}} \qquad (B.6)$$

APPENDIX C

Derivation of Electron Density and Collision Frequency From Attenuation and Phase Shift

The theory of the propagation of an electromagnetic wave through an ionized medium has been considered extensively at many levels. It shall be sufficient here to review the previous work in order to discuss the salient points encountered during this study. The starting point for the derivation of the theory is the Maxwell equations which are manipulated into the following form:

$$\frac{\partial^2 \bar{E}}{2\eta^2} - \mu \epsilon \frac{\partial^2 \bar{E}}{\partial t^2} - \mu \sigma \frac{\partial \bar{E}}{\partial t} = 0 \qquad \text{(C.1)}$$

where:

ϵ = capacitivity

μ = permeability

σ = conductivity

η = coordinate direction in which plane wave is travelling

$\bar{E}$ = electric field intensity

For a harmonic field variation, $e^{j\omega t}$, the solution to the electric field wave equation is:

$$\bar{E} = \bar{E}_o e^{-\gamma\eta} e^{j\omega t} \qquad \text{(C.2)}$$

The parameter γ is called the propagation constant and is defined as:

$$\gamma^2 = \mu \epsilon \omega^2 + j \mu \sigma \omega \qquad \text{(C.3)}$$

We now define,

$$\gamma = \alpha + j \tag{C.4}$$

and by solving equations (C.3) and (C.4) simultaneously, we obtain

$$\alpha = \omega \sqrt{\mu \epsilon} \left[\frac{\sqrt{1 + \frac{\sigma^2}{\epsilon^2 \omega^2}} + 1}{2} \right]^{1/2} \tag{C.5a}$$

$$\beta = \omega \sqrt{\mu \epsilon} \left[\frac{\sqrt{1 + \frac{\sigma^2}{\epsilon^2 \omega^2}} - 1}{2} \right]^{1/2} \tag{C.5b}$$

Equation (C.2) could now be written as:

$$\bar{E} = E_o e^{-\alpha \eta} e^{-j(\omega t - \beta \rho)} \tag{C.6}$$

to show that the solution contains a damping or attenuation term and a phase lag.

It is conventional to define the propagation constants in terms of an effective dielectric constant, defined as:

$$K = 1 + \frac{\sigma}{j \omega \epsilon} = K_r + j K_i \tag{C.7}$$

The propagation constants can then be written as:

$$\alpha = k \left(\frac{K - Kr}{2} \right)^{1/2} \tag{C.8a}$$

$$\beta = k \left(\frac{K + Kr}{2} \right)^{1/2} \tag{C.8b}$$

The conductivity, σ, can be evaluated from the solution to the force equation given below:

$$m_e \frac{dv}{dt} = m_e A(t) = - e E e^{jwt} \tag{C.9}$$

The extra force is due to elastic collisions of a charged particle with the molecules of the gas. The function, A(t), cannot be specified however, the time-averaged value can be considered as a damping force proportional to the electron velocity,

$$\overline{A(t)} = -\nu U \tag{C.10}$$

The proportionality constant, ν, has the dimensions of inverse time and is considered physically as a collision frequency for momentum transfer. The solution to equation (C.9) is given as:

$$U = \frac{-e E_o e^{j\omega t}}{m_e} \quad \left(\frac{1}{\nu + j\omega}\right) \tag{C.11}$$

The current density is defined as:

$$J = -n_e e U \frac{n_e e^2 E_o e^{j\omega t}}{m_e (\nu + j\omega)} \tag{C.12}$$

and the complex conductivity as:

$$\sigma = \sigma_r + j\sigma_i = \epsilon \omega_p^2 \frac{1}{(\nu + j\omega)}$$

where:

$$\omega_p^2 = \frac{n_e e^2}{\epsilon m_e}$$

The plasma frequency and collision frequency is normalized by the propagation frequency as follows:

$$N = \left(\frac{\omega_p}{\omega}\right)^2$$

$$S = \left(\frac{\nu}{\omega}\right)$$

The plasma dielectric constant written as functions of the normalized plasma frequency and collision frequency is given below.

$$K = 1 = N\left(\frac{1}{1 + S^2}\right) - j\,N\left(\frac{S}{1 + S^2}\right) \qquad (C.16)$$

The real and imaginary parts are given as

$$Kr = 1 - N\left(\frac{1}{1 + S^2}\right)$$

$$Ki = -N\left(\frac{1}{1 + S^2}\right)$$

In the laboratory, the plasma was bounded by dielectric windows so that the microwave signal entered and left the plasma through windows and boundary layers. The interface between the air and window and the window and plasma can introduce large effects on the transmitted signal and its phase. Bachynski (Reference 3) derived the following solution for the plasma slab bounded by dielectric plates.

If the dielectric plates are considered lossless, the impedance of the dielectric, Z_1, and the plasma, Z_2, can be written as:

$$Z_1 = \frac{Z_o}{K_1} = \frac{Z_o}{\mu}$$

$$Z_2 = \frac{Z_o}{\sqrt{K_2}} = Z_o\left(\frac{jk}{\alpha + j\beta}\right)$$

where:

Z_o = Freespace Impedance, 376.6 ohms

μ = Index of Refraction of the Dielectric Plate

k = Freespace Wave Number, $2\pi c/\omega$.

Bachynski defines:

$$Z_r\,(m = m) = \frac{1}{2}\left(\frac{1}{m}\right)\left(\frac{\beta}{k}\right)\frac{(m^2 + |k|)}{k}$$

$$Z_i\,(m = m) = \frac{1}{2}\left(\frac{1}{m}\right)\left(\frac{\alpha}{k}\right)\left(\frac{m^2 - |k|}{k}\right)$$

for $m = 1,\ \mu,$ or μ^2.

The transmission coefficient can be put in the following form

$$T = \frac{1}{A + j\,B}$$

where:

$$A = E' \cosh \alpha\, d \cos \beta\, d + F \sinh \alpha\, D \sin \beta\, d + C \sin L\, \alpha\, D \cos d - D \cosh \alpha\, d \sin \beta\, d$$

$$B = -F \cosh \alpha\, d \cos \beta\, d + E' \sin \alpha\, D \sin \beta\, d + D \sin L\, \alpha\, D \cos \beta\, d + c \cosh \alpha\, d \sin \beta\, d$$

$$C = -Z_{i(m=\mu)} \sin^2 \beta'\, d' + Z_{r(m=1)} \cos^2 \beta'\, d' - Z_{r(m=\mu^2)} \sin^2 \beta\, d'$$

$$D = Z_{r(m=\mu)} \sin^2 \beta\, d' + Z_{i(m=1)} \cos^2 \beta\, d' - Z_{i(m=\mu^2)} \sin^2 \beta\, d'$$

$$E' = \cos 2\beta\, d'$$

$$F = -\frac{1}{2}\left(\mu + \frac{1}{\mu}\right) \sin 2\beta\, d'$$

The attenuation and phase are expressed as:

$$\text{Attenuation} = 10 \log_{10} (A^2 + B^2)$$

$$\text{Phase} = \tan^{-1}\left(\frac{B}{A}\right)$$

The plexiglass windows used in the nozzle had a thickness of 0.50 inches and a refractive index of 1.66. The windows were spaced 1.50 inches apart. The optical path length in each window was 0.83 wavelength.

Numerical computation were made for the experimental test conditions with the above window parameters. The computed attenuation and phase shift as functions of the normalized plasmas and collision frequency are shown in Figure 9. The phase shift was adjusted for no phase shift when the electron density was zero. Similarly, the attenuation was adjusted to read zero in the absence of electrons.

REFERENCES

1. Hansen, C. Frederick, "Approximation for the Thermodynamic and Transport Properties of High-Temperature Air". NACA TN 4150, March 1958.

2. Mirels, Harold, "Shock Tube Test Time Limitations Due To Turbulent-Wall Boundary Layer". AIAA 2 84-93 (1964).

3. Bachynski, M. P., Cloutier, G. G., and Graf, K. A. "Microwave Measurements of Finite Plasmas"AFCRL 63-161, May 1963.

4. Bachynski, M. P., Johnson, T. W., and Shkaropky, J. P. "Electromagnetic Properties of High-Temperature Air". Proc. I. R. E., Vol. 48, pp 347 - 356, March (1960).

5. Musal, Henry, M. Jr. "Electron Collision Frequency in Equilibrium High Temperature Air". Bendix Corporation Research Note 9, May 1960, ASTIA 268 806.

6. Friel, P. J. and Rosenbaum, B. "Propagation of Electromagnetic Waves Through Re-Entry-Induced Plasmas". American Astronautical Society Preprint 62-18.

7. Lin, S. C. "Ionization Phenomenon of Shock-Waves in Oxygen-Nitrogen Mixtures". AVCO-Everett Research Report 33, June 1958.

8. Frost, A. A. and Peason, R. G. Kinetics and Mechanisms John Wiley and Sons, Inc. 1962.

NASA-Langley, 1966 CR-516